Pergamon

Int. J. Heat Mass Transfer. Vol. 39, No. 3, pp. 467–478, 1996

0017-9310/96 $9.50+0.00

0017-9310(95)00154-9

Steady natural convection in a double layer of immiscible liquids with density inversion

J. N. KOSTER† and KY NGUYEN

Department of Aerospace Engineering Sciences, University of Colorado Boulder, CO 80309-0429, U.S.A.

(*Received* 10 *January* 1995 *and in final form* 6 *April* 1995)

Abstract—Natural convection of a layered fluid system composed of two immiscible liquids, silicone oil on top of water, is studied numerically. The flow in the two layers is viscously and thermally coupled. Two counter-rotating natural convection roll cells of opposite vorticity develop when one side wall temperature in the density inversion fluid is above and the other below the density inversion temperature. In contrast, only one roll cell develops in a liquid layer with Boussinesq properties. The viscous coupling between both immiscible layers strengthens the roll cell with opposite vorticity in the density inversion layer. At large Rayleigh number the flow pattern in the density inversion layer becomes very complex. The largest heat transport occurs in the upper Boussinesq layer. The two-roll cell pattern in the density inversion layer is impeding the total horizontal heat transfer. A vertical heat transport exists across the interface from the density inversion layer into the encapsulating upper layer. The moving interface between the immiscible liquids improves the heat transfer in each layer when compared to the cavity cases.

INTRODUCTION

During solidification of electronic materials, thermal convection flow within the melts may cause undesirable crystallographic inhomogeneities in the solidified materials. A technique of liquid encapsulated crystal growth has been used to reduce component evaporation and thus non-stoichiometric solidification within the melt, with the ultimate goal to produce defect-free mono-crystalline electronic material. As a demonstration of this technique, germanium, PbTe, PbSe and GaAs single crystals were encapsulated with molten B_2O_3 as the confining liquid. [1, 2] Barocela and Jalilevand [3] suggested the method of liquid encapsulated float zone processing of GaAs in space. Doi and Koster [4] proposed to use the liquid encapsulation to control surface tension driven flow in a low-gravity environment. Recently, Prakash and Koster [5] studied analytically in great detail the coupling of immiscible multiple fluid layers without density inversion. Géoris *et al.* [6] analyzed the Marangoni–Bénard instability for symmetrical immiscible three-layer Boussinesq systems.

Some liquids do not necessarily obey Boussinesq assumptions, i.e. linearly changing thermophysical properties. The pseudobinary electronic alloy $Hg_{1-x}Cd_xTe$ does exhibit a density inversion at 1028 K, just above the melting temperature. Antar [7] did study several of the convection issues of $Hg_{1-x}Cd_xTe$, although his concern was the heating from below case. Campbell and Koster [8] found indications that the material gallium may also have a density inversion close to the melting temperature. Water is a more commonly known liquid that exhibits a density inversion in its liquid phase. This problem was studied rather extensively and we refer only to a few studies. Watson [9] analyzed the density inversion in a square vessel. Seki *et al.* [10] investigated a similar case and extended the temperature range. Robillard and Vasseur [11] studied transient effects. Lin and Nansteel [12] refined the knowledge of the flow structure with density inversion. Tong and Koster studied non-Boussinesq density fluid single layer steady-state natural convection [13, 14] as well as the transient case [15].

In this paper, we extend the research to study natural convection in the double immiscible liquid layer with density inversion present in the lower layer. This case is relevant to liquid encapsulation of an electronic material with density inversion, or to the environmental problem of oil spills on water. Of interest is the flow pattern and heat transfer when the density inversion temperature is in between the hot and cold side walls.

PHYSICAL MODEL

We study natural convection in a two-dimensional (2D) box filled with a Boussinesq fluid (silicone oil, 2 cSt) as top layer, and a density inversion fluid (water) at the bottom. Both fluids are enclosed in a $A = H/L = 2$ rectangular cavity (Fig. 1). The aspect ratio of each individual layer is one. The right wall is cold and its temperature, T_c, is kept constant and fixed below the density inversion point. The left side wall is heated at T_h and kept at, or above, the density inversion temperature T_0. The temperature difference between the two side walls is increased by increasing the hot side temperature T_h.

NOMENCLATURE

$A = H/L$	aspect ratio
g	gravitational acceleration
H	cavity height
h	heat transfer coefficient
k	thermal conductivity
L	cavity width
Nu	Nusselt number
P	nondimensional pressure
Pr	Prandtl number
R	density distribution parameter
Ra	Rayleigh number
T	temperature
U, V	nondimensional velocities
u, v	dimensional velocity
X, Y	nondimensional lengths
x, y	dimensional lengths.

Greek symbols

θ	nondimensional temperature
ρ	density
β	thermal expansion coefficient for Boussinesq fluid
γ	thermal expansion coefficient for density inversion liquid
μ	dynamic viscosity.

Subscripts

c	cold
h	hot
i	interface
j	variable referring to layer
0	reference value, density inversion point
1	lower density inversion layer
2	upper Boussinesq layer.

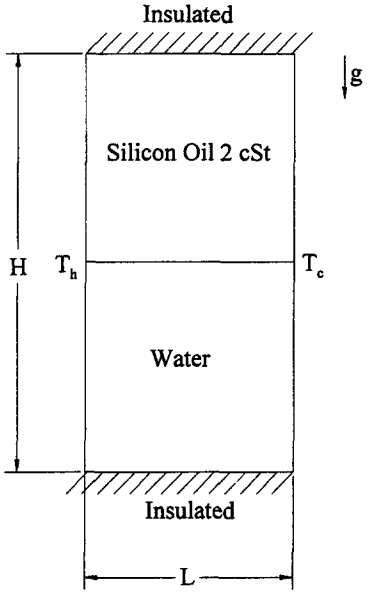

Fig. 1. Sketch of test cell and boundary conditions.

MATHEMATICAL FORMULATION

In the bottom water layer, the density inversion occurs at $T_0 = 3.98°C$. The right wall is kept below the density inversion point at a constant cold temperature of $T_c = 1°C$. The left wall temperature is varied from $3.98°C < T_h < 10°C$. The heated and cooled side walls are perfectly conducting and their temperature is uniform. Both top and bottom walls are thermally insulated. Two liquid regions are formed within the bottom layer in which $d\rho/dT > 0$ in the colder section of the layer, and $d\rho/dT < 0$ in the hotter section above the density inversion point.

The fluid motion is governed by the steady, incompressible Navier–Stokes and energy equations. For the bottom fluid:

$$\frac{\partial U_1}{\partial X} + \frac{\partial V_1}{\partial Y} = 0 \tag{1}$$

$$U_1 \frac{\partial U_1}{\partial X} + V_1 \frac{\partial U_1}{\partial Y} = -\frac{\partial P_1}{\partial X} + Pr_1 \left(\frac{\partial^2 U_1}{\partial X^2} + \frac{\partial^2 U_1}{\partial Y^2} \right) \tag{2}$$

$$U_1 \frac{\partial V_1}{\partial X} + V_1 \frac{\partial V_1}{Y} = -\frac{\partial P_1}{\partial Y} + Pr_1 \left(\frac{\partial^2 V_1}{\partial X^2} + \frac{\partial^2 V_1}{\partial Y^2} \right) + Ra_1 Pr_1 \theta_1^2 \tag{3}$$

$$U_1 \frac{\partial \theta_1}{\partial X} + V_1 \frac{\partial \theta_1}{\partial Y} = \frac{\partial^2 \theta_1}{\partial X^2} + \frac{\partial^2 \theta_1}{\partial Y^2} \tag{4}$$

where θ, P, (X, Y), (U, V) are the nondimensionalized temperature, pressure, lengths and velocities. The index 1 refers to the lower layer, index 2 refers to the upper layer. Similarly, for the Boussinesq top fluid with linear density profile, we have:

$$\frac{\partial U_2}{\partial X} + \frac{\partial V_2}{\partial Y} = 0 \tag{5}$$

$$U_2 \frac{\partial U_2}{\partial X} + V_2 \frac{\partial U_2}{\partial Y} = -\frac{\partial P_2}{\partial X} + Pr_2 \left(\frac{\partial^2 U_2}{\partial X^2} + \frac{\partial^2 U_2}{\partial Y^2} \right) \tag{6}$$

$$U_2 \frac{\partial V_2}{\partial X} + V_2 \frac{\partial V_2}{\partial Y} = -\frac{\partial P_2}{\partial Y} + Pr_2 \left(\frac{\partial^2 V_2}{\partial X^2} + \frac{\partial^2 V_2}{\partial Y^2} \right) + Ra_2 Pr_2 \theta_2 \tag{7}$$

$$U_2\frac{\partial\theta_2}{\partial X}+V_2\frac{\partial\theta_2}{\partial Y}=\frac{\partial^2\theta_2}{\partial X^2}+\frac{\partial^2\theta_2}{\partial Y^2} \tag{8}$$

where the thermal expansion coefficient in the liquid with density inversion is calculated as $\gamma = 8.0\times10^{-6}(°C)^{-2}$ and ρ_0 is the maximum density at the temperature $T_0 = 3.98°C$. The parabolic density–temperature relationship is given as

$$\frac{\rho}{\rho_0}=1.0-\gamma(T-T_0)^2. \tag{9}$$

This correlation has been widely used and, as discussed by Tong and Koster [14], the correlation provides sufficient accuracy for the proposed range of temperatures.

The governing equations, expressing conservation of mass, momentum, and energy, based on the assumption of constant fluid properties except for the density in the body force term, are non-dimensionalized using the following variables:

$$U_j=\frac{u_jL}{\kappa_j};\quad V_j=\frac{v_jL}{\kappa_j};\quad j=1,2$$

$$X=\frac{x}{L};\quad Y=\frac{y}{L}$$

$$P_j=\frac{p_j}{\rho_j\left(\frac{\kappa_j}{L}\right)^2}\quad j=1,2$$

$$\theta_j=\frac{T_j-T_0}{\Delta T}\quad j=1,2\quad \Delta T=T_h-T_c$$

The Rayleigh and Prandtl numbers are defined for the individual layers as:

$$Ra_1=\frac{g\gamma(\Delta T)^2L^3}{\kappa_1\nu_1};\quad Ra_2=\frac{g\beta(\Delta T)L^3}{\kappa_2\nu_2} \tag{10}$$

$$Pr_j=\frac{\nu_j}{\kappa_j}\quad j=1,2. \tag{11}$$

The Prandtl number of water is fixed at $Pr_1 = 11.57$. The Prandtl number of the silicone oil is $Pr_2 = 27.5$. Note that the Rayleigh number for the density inversion layer [equation (10)] is based on the horizontal temperature difference ΔT^2 and $\gamma(°C^{-2})$, rather than ΔT and $\beta(°C^{-1})$ as in traditional Boussinesq cases.

Lin and Nansteel [12] defined the following density distribution parameter:

$$R=\frac{T_0-T_c}{T_h-T_c} \tag{12}$$

which describes the location of the density inversion temperature with respect to the sidewall temperatures.

The governing equations (1)–(8) are subjected to no-slip boundary conditions at all side walls, constant temperatures at the vertical walls and adiabatic conditions at the horizontal walls. Temperature and velocity boundary conditions at the liquid–liquid interface are obtained from the stress balance, heat flux balance and velocity and temperature continuity at the interface:

$$\mu_1\frac{\partial u_1}{\partial y}=\mu_2\frac{\partial u_2}{\partial y} \tag{13}$$

$$k_1\frac{\partial T_1}{\partial y}=k_2\frac{\partial T_2}{\partial y} \tag{14}$$

$$u_1=u_2\quad T_1=T_2 \tag{15}$$

where μ is the dynamic viscosity, k the thermal conductivity, u and T the dimensional horizontal velocity and local temperature at the interface. Thermocapillarity effects are neglected in equation (13) as buoyancy is dominant.

NUMERICAL SIMULATION

The double layer problem is numerically simulated using the commercial finite element computer code FIDAP. The simulation is restricted to a two-dimensional model. The interface is considered to be slightly deformable. Deformation is so small (10^{-4} cm or 0.03% of cavity height) that it is neglected in the discussion. Thermocapillary effects are neglected as buoyancy effects are dominant. The interface is pinned at the side walls. The governing steady Navier–Stokes equations, the energy equation, along with the stress balance and kinematic condition at the interface are discretized using the finite element method. The discretized system is then solved using FIDAP's segregated technique. The mixed pressure approach is used for the pressure formulation. With the segregated algorithm, the free surface problem is solved in two steps. First a solution is sought by imposing the kinematic balance and, once the field variables are converged, the normal stress balance, without thermocapillary effects, is applied to define the movement of the interface. The procedure is repeated until full convergence is achieved. For a complete description of the discretization procedure and the solution methods available, we refer readers to the FIDAP users' manual [16].

The test mesh is of the dimension 105×57. A grid mesh study for a similar density inversion problem was done by Tong and Koster [14] which showed that a much smaller mesh size would be sufficient for high accuracy. The governing equations are solved in dimensional form. The mixed pressure parameter is set to 10^{-10}. The convergence criteria for the velocity norm is set to 10^{-5}, and 10^{-3} for the surface norm. For details on these parameters, we refer readers to the FIDAP manuals [16].

RESULTS AND DISCUSSION

Temperature field and convective flow pattern

Subject to any temperature difference a single roll convective flow will develop in the upper Boussinesq liquid layer. In the lower non-Boussinesq layer it is

necessary to consider the actual temperatures at the side walls and the location of the density inversion temperature within the bulk fluid. When both the hot and cold wall temperatures are above the density inversion temperature the flow in both layers is of same vorticity and an interfacial coupling roll develops between upper and lower layers [5]. In the case of a density inversion layer, with one side wall temperature below the density inversion temperature, the fluid rises at the cold wall and descends near the density inversion plane [13, 14]. A second roll cell develops with upflow at the hot side wall and downflow near the density inversion plane within the bulk. The definition proposed by Tong and Koster [13] of the "regular" and "inversional" convection rolls will be adopted here. The "regular" convection roll develops in the Boussinesq fluid as well as in the hotter section of the density inversion layer with $d\rho/dT < 0$. The opposite vorticity "inversional" convection roll develops in the section of the fluid layer with density inversion where $d\rho/dT > 0$.

In the numerical experiments the Rayleigh number of the density inversion layer is kept constant at, e.g. $Ra_1 = 10^3$ and the temperature difference is increased while reducing the length L and leaving the aspect ratio constant. This allows an assessment of the effect of density inversion at constant buoyancy driving force in that layer. Congruently, the density distribution parameter R and the Rayleigh number in the upper Boussinesq layer become smaller with increased temperature difference and reduced length L. Physically, this means the driving buoyancy force in the upper layer is decreased.

The cold side wall temperature is set in most cases to $T_c = 1°C$. At $\Delta T = 3$ K ($Ra_1 = 10^3$, $Ra_2 = 7.1 \times 10^4$, $R = 1$), which sets the hot side close to the density inversion temperature, the flow rising at the hot wall in the upper layer is well coupled to the flow descending at the hot wall in the lower density inversion layer (Fig. 2). The flow direction at the interface of both layers is in the same direction and both convection cells have opposite vorticity. The difference in Rayleigh number (strength of buoyancy driven flow) between the lower and upper layers is reflected by the visualized streamline contour plots.

As the temperature at the hot wall becomes higher than $T_h = 3.98°C$, the maximum density temperature of water, a "regular" convective roll develops with rising flow at the hot wall. At $Ra_1 = 10^3$ and $\Delta T = 5$ K ($T_h = 6°C$, $Ra_2 = 4.3 \times 10^4$, $R = 0.6$), this very small "regular" convective roll is confined to the lower left corner. The maximum density temperature plane ($\theta = 0$, $T_0 = 3.98°C$) is shown across the flow pattern in the lower layer and extended into the upper layer, starting at the vertical left wall when $T_h = T_0 (R = 1)$. As observed by Tong and Koster [13] for the single layer, the "inversional" convective roll penetrates across the density maximum temperature plane $\theta = 0$.

With decreasing density distribution parameter R and Rayleigh number Ra_2 the flow pattern in the upper fluid remains qualitatively the same but becomes weaker. The maximum density plane ($\theta = 0$) in the lower layer shifts to the right and the "regular" convective roll grows bigger. Due to strong viscous coupling between the top layer roll (of "regular" type and vorticity) and the bottom layer "inversional" roll, the "regular" convective cell of the density inversion fluid remains confined to the lower left corner and grows as the strength of the convective flow in the encapsulant is reduced. This flow pattern is different in the single layer inversional case [13] where both rolls extend from bottom to top of the liquid layer.

Note the different profile of the $\theta = 0$ line in the upper and lower layers. The "inversional" roll cell penetrates at all times across the $\theta = 0$ line and is enhanced by the viscous coupling to the upper roll. The temperature profiles indicate that the interface is not adiabatic, which will be addressed later.

At higher Rayleigh number, $Ra_1 = 10^4$ (Fig. 3), a similar flow pattern development is realized at large R-value. Due to the geometry change, the strength of the buoyancy roll in the upper layer is reduced as ΔT increases. At $Ra_2 = 4.3 \times 10^5$ and $R = 0.6$ ($\Delta T = 5$ K) a "regular" convection cell has developed in the lower left corner of the density inversion fluid. At $R = 0.375$ ($\Delta T = 8$ K) the "inversional" roll cell breaks up into two smaller roll cells. Both cells continue to rotate counter-clockwise, thus retaining their "inversional" character. One of the "inversional" rolls takes over the role as the *interfacial coupling* roll cell between the lower and the upper liquid layers (see [5]). As this "inversional" roll is driven by buoyancy forces its size and shape is much different to the shear-induced coupling roll cell of two immiscible Boussinesq liquids. Note that after the breakup the "inversional" roll at the interface penetrates substantially across the $\theta = 0$ line. This penetration distance is made possible by the viscous coupling to the upper layer. At lower $R = 0.33$ (also lower Ra_2-value), the "regular" roll cell in the density inversion fluid also penetrates across the $\theta = 0$ line. Decreasing R further will squeeze the smaller second "inversional" roll cell into the lower right corner. The reduced buoyancy force in the upper layer has a lesser effect on the lower layer convection, which strengthens the "regular" cell.

At the higher Ra_1-number cases the horizontal thermal stratification in the top Boussinesq fluid becomes, as expected, more pronounced as the flow adopts the typical boundary layer flow pattern. The lower layer does not develop an equivalent thermal stratification pattern as the buoyancy force is relatively small.

As the Rayleigh number is increased further, the breaking up of the "inversional" cell in the lower layer occurs more readily. The higher Ra_1 strengthens the "regular" roll cell substantially.

Heat transfer at vertical walls

Local and average Nusselt numbers give insight in the heat transfer mechanism of convective flow

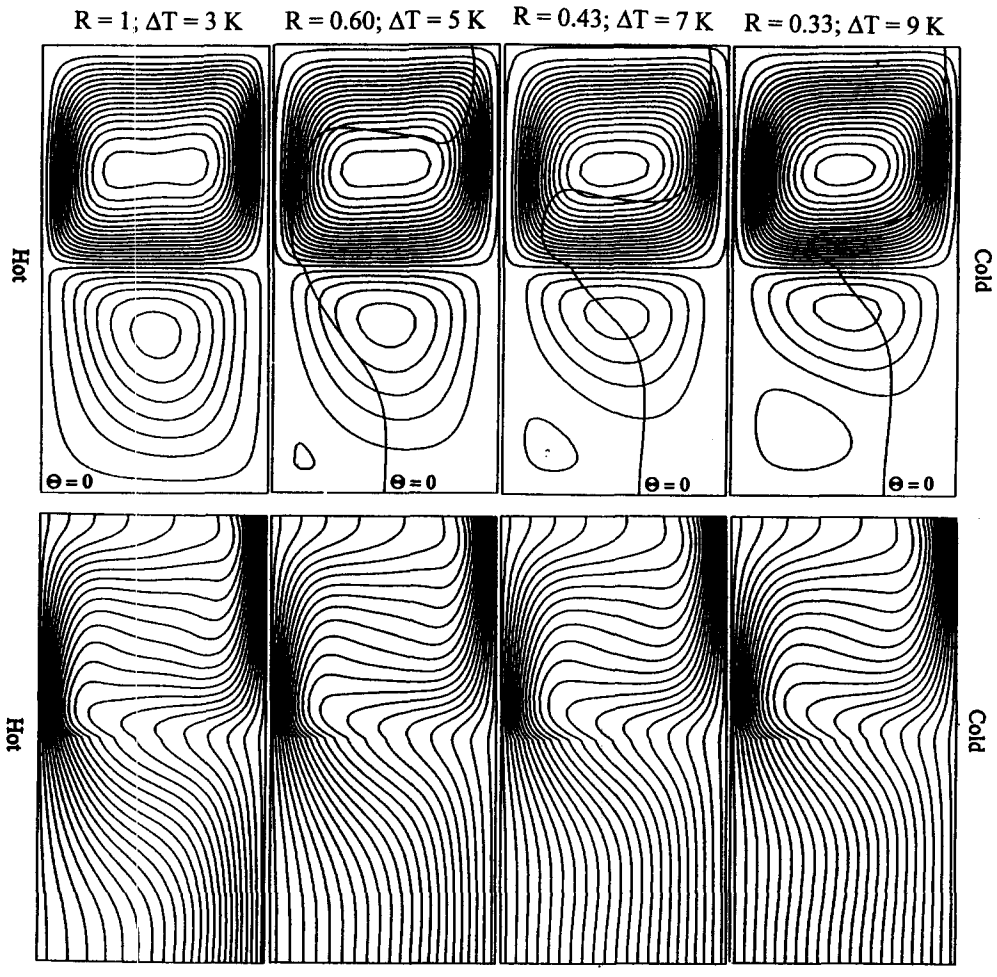

Fig. 2. $Ra_1 = 10^3$: streamline (top) and temperature (bottom) contours at various temperature gradients. $10^{-4}\, Ra_2 = 7.1, 4.3, 3.1, 2.4$. The maximum density plane ($\theta = 0$) is added to show visually the penetration of the flow across this plane.

situations. The local Nusselt number at vertical walls is defined as:

$$Nu_y = \frac{hL}{k} \tag{16}$$

where the heat transfer coefficient h is defined as:

$$h = \frac{k}{\Delta T}\left|\frac{\partial T}{\partial x}\right|_{x=0,\,x=L}. \tag{17}$$

In terms of nondimensional variables, the local Nusselt number can also be expressed as:

$$Nu_y = \left|\frac{\partial \theta}{\partial X}\right|_{X=0,\,X=1}. \tag{18}$$

The average Nusselt number is then obtained by integrating the local Nusselt number along the vertical walls (e.g. at the hot wall):

$$\overline{Nu} = \frac{1}{(H/L)}\int_0^{(H/L)}\left|\frac{\partial \theta}{\partial X}\right|_{X=0} \mathrm{d}. \tag{19}$$

The local Nusselt number profile in the upper Boussinesq layer is similar to single layer case profiles, except that the profile is distorted close to the interface to accommodate the thermal coupling across the interface with the lower layer (Fig. 4). The "inversional" roll does reduce the heat transport in the neighborhood of the interface. In the lower layer close to the interface the Nusselt number at the hot wall is relatively high, and becomes very low as the lower bottom is neared. This pattern is due to the strong flow of the "inversional" roll, which wets both the left and right side walls, in comparison to the very weak flow in both the lower left and right corners. As R is decreased (ΔT increased), the hot and cold wall local Nusselt number curves are converging to $Nu_y = 1$ near the bottom of the test cell ($R = 0.30$, $\Delta T = 10$ K, $Ra_2 = 2.1 \times 10^4$).

The averaged heat transfer in the lower (Nu_1) and upper (Nu_2) layers are different; less heat is transported through the density inversion layer. With constant Ra_1-number and decreasing R-number and Ra_2-number the average total (as well as averaged individual layer) heat transfer is reduced. No distinct

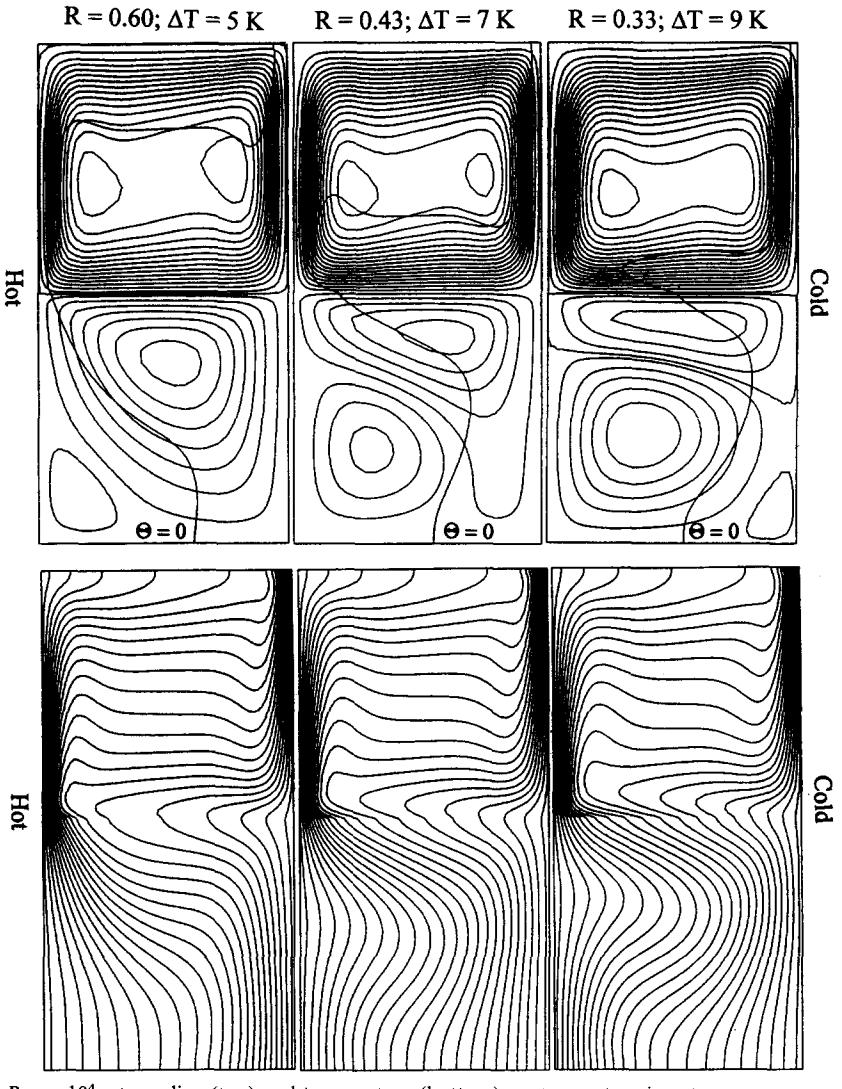

Fig. 3. $Ra_1 = 10^4$: streamline (top) and temperature (bottom) contours at various temperature gradients. 10^{-5} $Ra_2 = 4.3, 3.1, 2.4$. The maximum density plane ($\theta = 0$) is added to show visually the penetration of the flow across this plane.

change in heat transfer profile as a function of applied temperature difference, or R-value, is observed in the upper layer.

Plots of the average total Nusselt number across both layers at different Rayleigh numbers for various temperature differences are shown in Figs. 5(a)–(c). We observe that, for all Rayleigh numbers Ra_1, the overall (total) average Nusselt number for the double layer [Fig. 5(a)] is always decreasing with decreasing R and Ra_2. The trend is different from the behavior of the single density inversion layer [13] where the heat transfer rebounds at $R = 0.5$ (symmetric density case, $\Delta T = 8$ K for $T_c = 0°C$). Looking at the heat transfer at the side walls of the lower density inversion layer [Fig. 5(b)] does however show for $R = 0.5$ ($Ra_2 = 3.6 \times 10^6$), at higher Rayleigh number $Ra_1 = 10^5$, a similar rebound in Nusselt number as found for the single layer. At smaller Ra_1 the coupling with the upper layer substantially affects the heat transfer in the density inversion layer. There is also a difference in local heat transfer between the hot wall and cold wall [Fig. 5(c)]. The difference is due to thermal coupling of both immiscible layers and is discussed later.

Figure 6 shows that at higher Rayleigh number ($Ra_1 = 10^4$) the two Nu-curves for the hot and cold walls start to cross-over a second time when R is reduced from 0.60 to 0.43. Most of the heat transfer in the density inversion layer happens close to the interface. The same trend in reduction of Nusselt number as a function of increased temperature difference is observed, confirming the influence of the "inversional" convection cell. At $Ra_1 = 10^5$, Fig. 7, the second crossing occurs even at a higher R-value ($\Delta T = 6$ K, $Ra_2 = 3.6 \times 10^6$, $R = 0.5$). This characteristic behavior reflects and is a consequence of the splitting of the "inversional" roll.

Figure 8 gives a general view of how the local Nus-

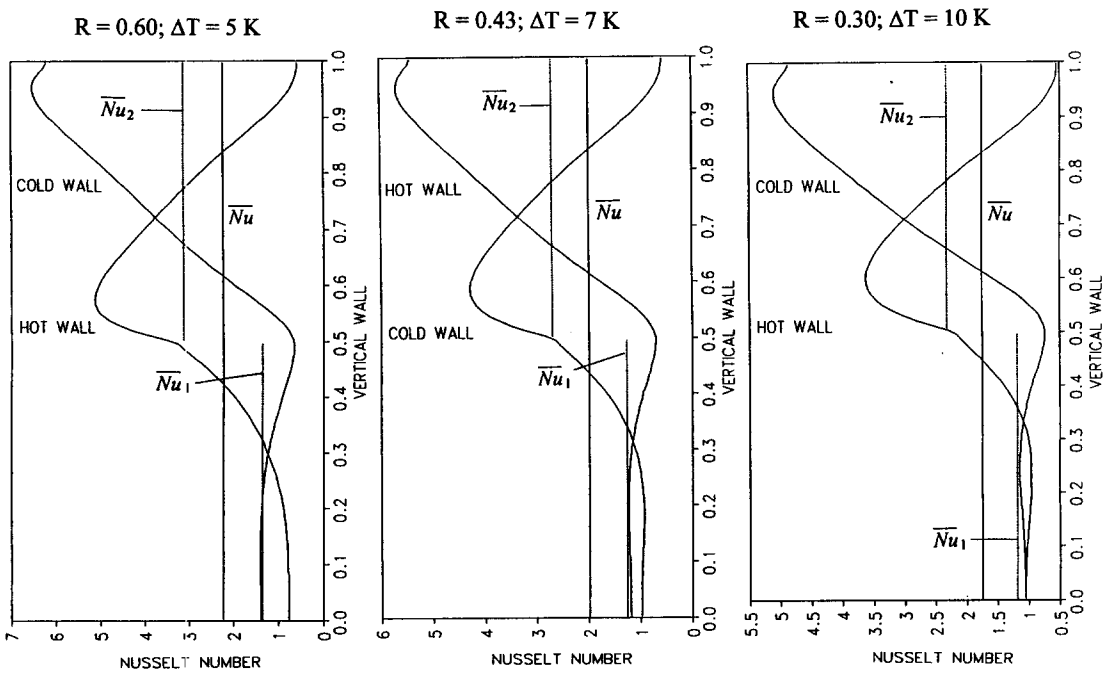

Fig. 4. Local and average Nusselt profile for $Ra_1 = 10^3$ at different temperature gradients (10^{-4} $Ra_2 = 4.3$, 3.1, 2.1). $\overline{Nu}_1$ = average, density inversion layer, $\overline{Nu}_2$ = average, Boussinesq layer, $\overline{Nu}$ = average, combined double layer (hot wall values).

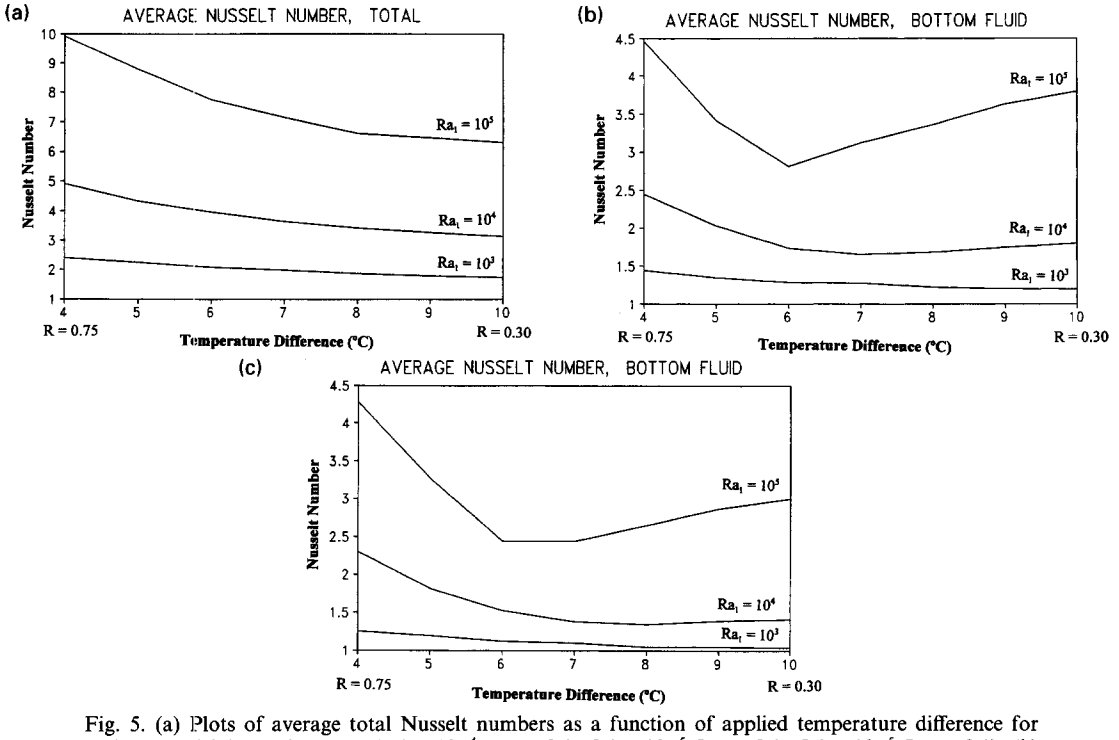

Fig. 5. (a) Plots of average total Nusselt numbers as a function of applied temperature difference for various Rayleigh numbers Ra_1 ($5.4 < 10^{-4}\ Ra_2 < 2.1$; $5.4 < 10^{-5}\ Ra_2 < 2.1$; $5.4 < 10^{-5}\ Ra_2 < 2.1$). (b) Average heat transfer at the hot wall in the density inversion layer as a function of temperature difference and Rayleigh number Ra_1. (c) Average heat transfer at the cold wall in the density inversion layer as a function of temperature difference and Rayleigh number Ra_1.

selt number evolves with temperature difference and R-value for different Rayleigh numbers Ra_1. At three Rayleigh numbers Ra_1 the development of the cold and hot wall local Nusselt numbers are displayed. The heat transfer in the lower density inversion layer is in general much smaller than the heat transfer in the

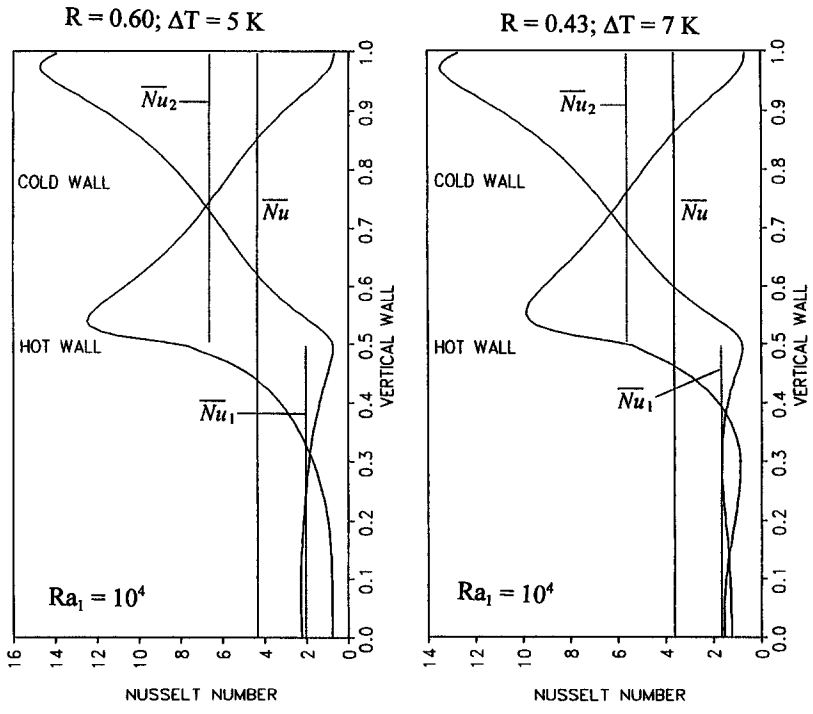

Fig. 6. Local and hot wall average Nusselt profile for single and both layers at $Ra_1 = 10^4$ and different temperature gradients (10^{-5} $Ra_2 = 4.3, 3.1$).

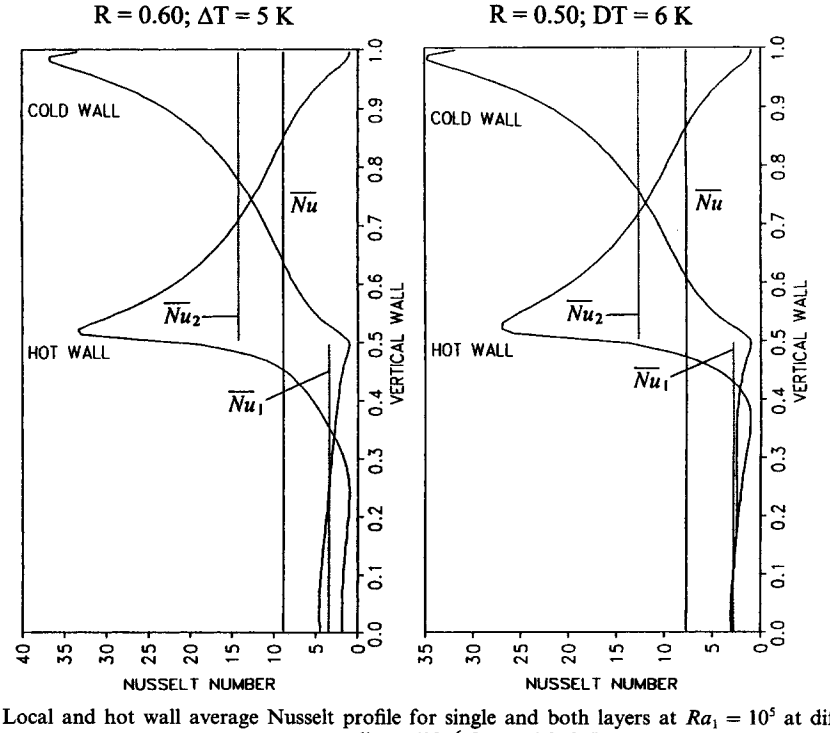

Fig. 7. Local and hot wall average Nusselt profile for single and both layers at $Ra_1 = 10^5$ at different temperature gradients (10^{-6} $Ra_2 = 4.3, 3.6$).

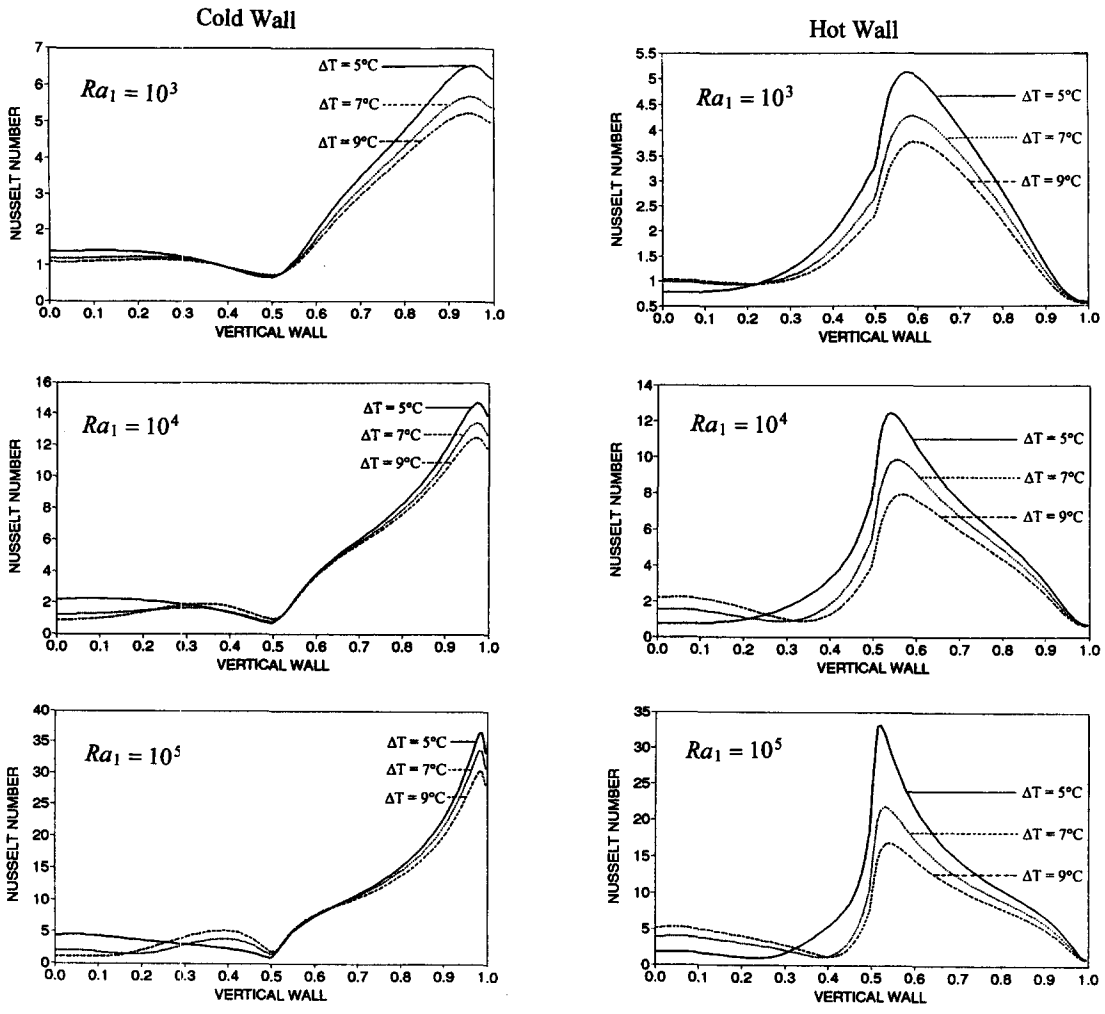

Fig. 8. Local Nusselt profiles for cold wall (left) and hot wall (right) for different Rayleigh numbers and temperature differences: $\Delta T = 5°C$ ($R = 0.60$); $\Delta T = 7°C$ ($R = 0.43$); $\Delta T = 9°C$ ($R = 0.33$). (10^{-4} $Ra_2 = 4.3, 3.1, 2.4$; 10^{-5} $Ra_2 = 4.3, 3.1, 2.4$; 10^{-6} $Ra_2 = 4.3, 3.1, 2.4$.)

upper Boussinesq layer despite the uniform temperature, T_h and T_c, along the side walls. The largest heat transport occurs in the upper layer which is subject to a higher Rayleigh number ($Ra_2 > Ra_1$) and also has a single, vigorously convecting roll cell (see Fig. 2). The lower layer two-roll pattern is impeding the heat transfer. The heat transfer profile is different at both heated/cooled walls. As the R-value and the Rayleigh number Ra_2 are reduced (temperature difference is increased), density inversion in one layer does reduce the heat transfer capability of a multilayer fluid system.

Comparing the average Nusselt numbers as a function of Rayleigh number Ra_1 and applied temperature difference demonstrates this contention (Fig. 9). Results from single square layer studies by Lin and Nansteel [12] are compared to the functional dependence of the heat transfer in the encapsulated immiscible liquid layer case, for the total Nusselt number, and for the Nusselt number at the side walls of the lower layer only. Here, for all calculations $T_c = 0°C$.

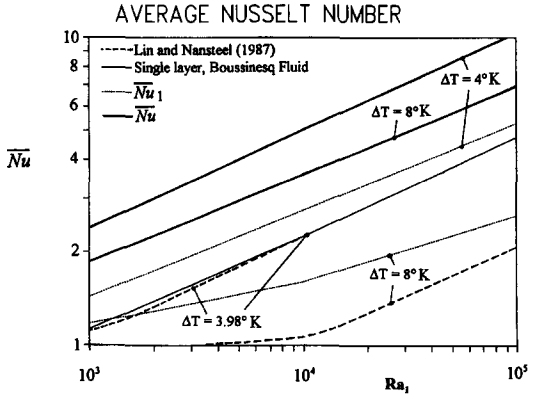

Fig. 9. Average heat transfer as a function of Rayleigh number Ra_1 for the single, individual and double layers as a function of density inversion contribution: $\Delta T = 4°C$ ($R = 1.00$); $\Delta T = 8°C$ ($R = 0.50$). (10^{-4} $Ra_2 = 5.4, 2.7$; 10^{-5} $Ra_2 = 5.4, 2.7$; 10^{-6} $Ra_2 = 5.4, 2.7$.)

The heat transfer for a Boussinesq fluid with linear heat transfer (water at room temperature) in a single square layer does, only at small Rayleigh numbers Ra_1, deviate slightly from the non-linear density profile case below the density inversion point. At $R = 1$, with the hot wall temperature close to the density inversion point ($5.4 < 10^{-4}\ Ra_2 < 5400$, $\Delta T = 4$ K), the heat transport through the encapsulated layer is much higher in the lower layer alone and in the combined double layer. This can be credited to the viscously well coupled moving interface in the double layer situation which eases the flow and consequently improves the heat transfer. The graph, however, indicates a trend that at higher Rayleigh number there might be less of a favorable heat transport in the encapsulated layer case. In the case of the symmetric density profile at $R = 0.50$ ($2.7 < 10^{-4} Ra_2 < 2700$, $\Delta T = 8$ K), the heat transport through the encapsulated layer remains superior to the single layer case of a density inversion layer, both for the individual density inversion layer and the double layer.

Heat transfer across the interface

The difference in horizontal heat transfer in the two viscously and thermally coupled liquid layers requires an evaluation of heat transfer across the interface between the two liquids. The local Nusselt number (in terms of nondimensional variables) at the interface is defined as:

$$Nu_i = \frac{\partial \theta}{\partial Y} \tag{20}$$

along the horizontal interface with a local vertical temperature gradient at the interface. Plots of the local Nusselt number along the interface at various horizontal temperature gradients and Rayleigh numbers are shown in Fig. 10. The total average Nusselt number value, shown at the right axis in Fig. 10, is positive for all cases studied. This indicates that there is always a positive net heat transport from the lower density inversion layer into the upper Boussinesq fluid. The highest vertical heat transfer is found close to the hot wall. This is because the "inversional" roll cell underneath the interface transports cold fluid toward the hot wall and thus reduces the heat transfer. As the Rayleigh number Ra_1 increases, the Nu-curves become sharper at their peaks, and flatter near the center of the interface which reflects the increased strength of the "inversional" convective flow at the interface in the bottom layer. The higher Ra_2 and R (lower temperature difference) the flatter becomes the Nusselt number curve along a large portion of the interface, as expected from the more vigorous flow in the upper layer. This heat transfer across the interface enhances the buoyancy convection in the upper layer.

SUMMARY AND CONCLUSION

Natural convective flow in a liquid encapsulated fluid layer with density inversion in the lower layer was studied numerically. The combined aspect ratio is $A = 2$ and the individual layer aspect ratio is $A = 1$. The goal was to obtain the flow pattern resulting from the viscous coupling of both layers and how they affect each other at different driving forces. As both layers are also thermally coupled, the density inversion does affect the overall heat transfer within each fluid and across the interface.

This study shows that the flow pattern is qualitatively and quantitatively different from the Boussinesq double layer case without density inversion. The flow pattern in the liquid encapsulated density inversion layer is also different to the flow pattern in the non-encapsulated single layer density inversion liquid. With one side wall temperature above the density inversion temperature there are always two counter-rotating rolls in the density inversion fluid. The viscous coupling between both layers strengthens the "inversional" roll cell even though buoyancy forces oppose that flow with a "regular" roll cell. "Regular" and "inversional" rolls are not side-by-side as in the single layer cavity case. The "inversional" roll is viscously coupled to the convecting upper liquid layer and serves as "interfacial" coupling roll with the buoyancy driven upper immiscible "regular" roll cell. The pattern of this roll is different from the shear-induced interfacial roll in the case where both immiscible liquids are Boussinesq with similar $\rho(T)$ dependence. The "regular" roll cell in the density inversion layer is more suppressed when the buoyancy force in the upper layer is high. As the buoyancy force in the encapsulant is reduced the "regular" roll tends to grow and splits the single "inversional" roll into two "inversional" roll cells.

Because of the heat transfer resistance emanating from the "regular" and "inversional" convection roll pattern in the density inversion layer the convective heat transport across the density inversion layer is less but locally more uniform than in the adjoining Boussinesq layer. This situation leads to a vertical heat transport from the density inversion layer into the encapsulating immiscible Boussinesq layer. The maximum vertical heat transfer across the interface occurs near the hot side wall which is explained by the heat transport of the inversional roll serving as an interfacial coupling roll cell.

In comparison to the single-layer density inversion case [14], no symmetric profiles in local Nusselt number, streamline, or temperature contour are obtained because of the mechanical coupling between both immiscible layers. The net heat transport through both layers individually is higher in the double layer case than through a single square cavity layer with or without density inversion. The moving interface improves the horizontal heat transport. The break-up of the "inversional" roll at higher Rayleigh number Ra_1 has a distinct effect on the local heat transfer: heat transfer profiles at the hot and cold sides are, over a larger vertical extension, smoothed and close in numerical value.

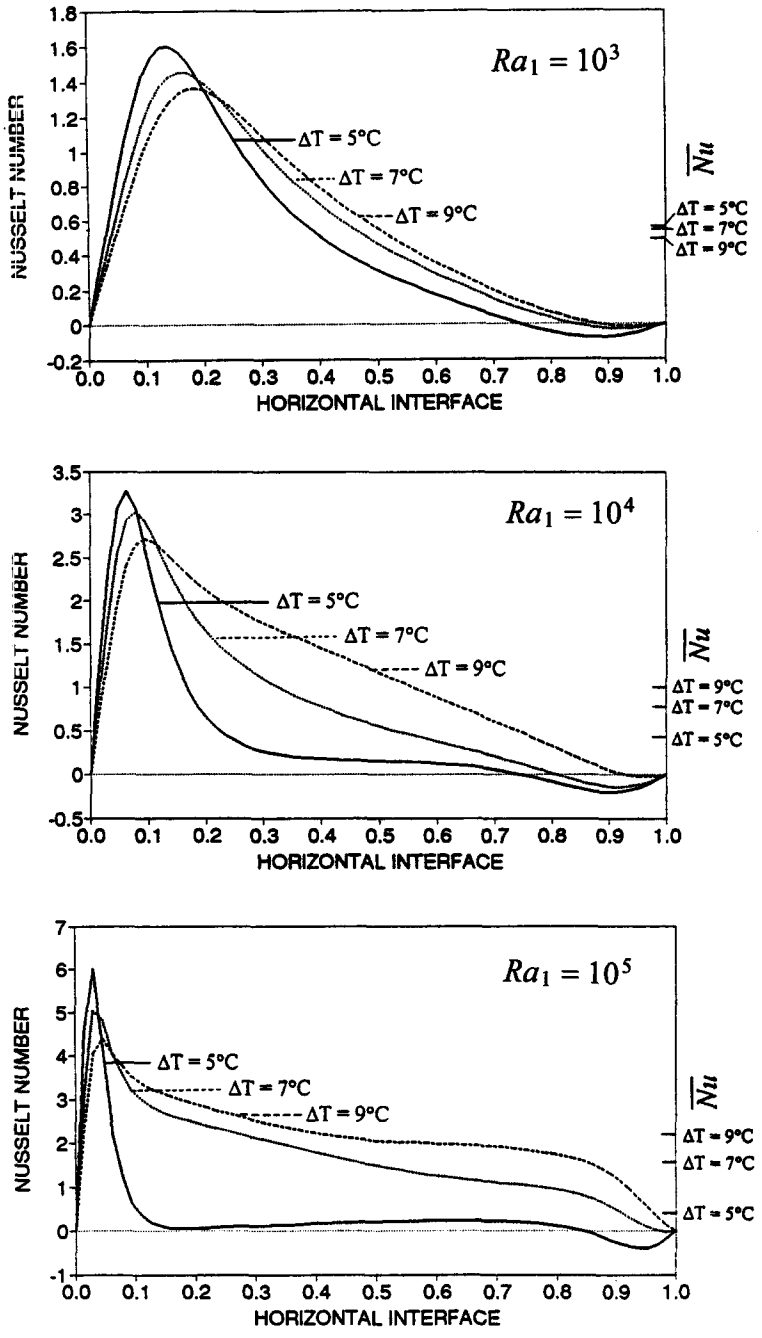

Fig. 10. Local Nusselt number across the interface for various Rayleigh numbers Ra_1: $\Delta T = 5°C$ ($R = 0.60$); $\Delta T = 7°C$ ($R = 0.43$); $\Delta T = 9°C$ ($R = 0.33$). (10^{-4} $Ra_2 = 4.3, 3.1, 2.4$; 10^{-5} $Ra_2 = 4.3, 3.1, 2.4$; 10^{-6} $Ra_2 = 4.3, 3.1, 2.4$.)

Table 1. Fluid properties

	Density ρ [g cm^{-3}]	Kinematic viscosity ν (cm^2 s^{-1})	Thermal conductivity k [cal cm^{-1} s^{-1} K^{-1}]	Specific heat c_p [cal g^{-1} K^{-1}]	Expansion coefficients β, γ
Silicone oil (2cSt)	0.871	2.00E−02	2.60E−04	4.10E−01	1.17E−03 (C^{-1})
Water	equation (11)	1.57E−02	1.36E−03	1.00	8.00E−06 (C^{-2})

Acknowledgement—Funding for this work provided by NASA MSAD under grant NAG3-1094 is gratefully acknowledged.

REFERENCES

1. E. P. A. Metz, R. C. Miller and R. Mazelsky, A technique for pulling single crystals of volatile materials, *J. Appl. Phys.* **33,** 2016–2017 (1962).
2. E. S. Johnson, Liquid encapsulated float zone melting of GaAs, *J. Cryst. Growth* **30,** 249–256 (1975).
3. E. Barocela and A. Jalilevand, Liquid encapsulated float zone method for microgravity production of gallium arsenide, AIAA paper 87-0390 (1987).
4. T. Doi and J. N. Koster, Thermocapillary convection in two immiscible liquids layers with free surface, *Phys. Fluids A* **5,** 1914–1927 (1993).
5. A. Prakash and J. N. Koster, Convection in multiple layers of immiscible liquids in a shallow cavity, *Int. J. Multiphase Flow* **20,** 383–396; 397–414 (1994).
6. Ph. Géoris, M. Hennenberg, I. B. Simanovskii, A. Nepomniaschy, I. I. Wertgeim and J. C. Legros, Thermocapillary convection in a multilayered system, *Phys. Fluids A* **5,** 1575–1582 (1993).
7. B. N. Antar, Convective instabilities in the melt for solidifying mercury cadmium telluride, *J. Crystal Growth* **113,** 92–102 (1991).
8. T. A. Campbell and J. N. Koster, Visualization of liquid–solid interface morphologies in gallium subject to natural convection, *J. Crystal Growth* **140,** 414–425 (1994).
9. A. Watson, The effect of the inversion temperature on the convection of water in an enclosed rectangular cavity, *Q. J. Mech. Appl. Math.* **25,** 423–446 (1972).
10. N. Seki, S. Fukusako and H. Inaba, Free convective heat transfer with density inversion in a confined rectangular vessel, *Wärme-und Stoffübertragung* **11,** 145–156 (1978).
11. L. Robillard and P. Vasseur, Transient natural convection heat transfer of water with maximum density and supercooling, *J. Heat Transfer* **103,** 528–534 (1981).
12. D. S. Lin and M. W. Nansteel, Natural convection heat transfer in a square enclosure containing water near its density maximum, *Int. J. Heat Mass Transfer* **30,** 2319–2329 (1987).
13. W. Tong and J. N. Koster, Coupling of natural convection flow across a vertical density inversion interface, *Wärme-und Stoffübertragung* **28,** 471–479 (1993).
14. W. Tong and J. N. Koster, Natural convection of water in a rectangular cavity including density inversion, *Int. J. Heat Fluid Flow* **14,** 366–375 (1993).
15. W. Tong and J. N. Koster, Density inversion effect on transient natural convection in a rectangular enclosure, *Int. J. Heat Mass Transfer* **37,** 927–938 (1994).
16. FIDAP, *Users' Manual.* Fluid Dynamics International, Evanston, IL (1993).